Iğdır Üniversitesi Fen Bilimleri Enstitüsü Dergisi, 12(3): 1477 - 1488, 2022
Journal of the Institute of Science and Technology, 12(3): 1477 - 1488, 2022

ISSN: 2146-0574, eISSN: 2536-4618

Electrical Electronic Engineering **DOI: 10.21597/jist.1132197**

Research Article

Received: 17.06.2022 **Accepted: 30.07.2022**

To Cite: Özçiflikçi O.E., Koç M., 2022. Investigations of hysteresis based direct torque controlled and field oriented controlled IPM drives for electric vehicle applications. Journal of the Institute of Science and Technology, 12(3): 1477 - 1488.

Investigations of hysteresis based direct torque controlled and field oriented controlled IPM drives for electric vehicle applications

Osman Emre ÖZÇİFLİKÇİ[1*], Mikail KOÇ[1]

ABSTRACT: Direct Torque Control (DTC) techniques are widely used in the control of AC machines as an opponent of space vector pulse width modulation (SVPWM) based field-oriented control (FOC). In the literature, hysteresis-based DTC (HB-DTC) is a vast majority of DTC techniques as the technique do not require a position resolver or an encoder. In this study, HB-DTC and FOC techniques are compared in detail by paying particular attention to current distortions, torque ripple and computational burden. In both techniques, the results have been obtained by simulating a 4.1 kW interior mounted permanent magnet synchronous (IPM) motor which has been designed and manufactured for research and development for electric vehicle traction applications. The results validate that although the HB-DTC drives, have pros such as having less computational burden on the processor and eliminating the need for a position sensor, they have relatively much current distortions and torque ripple and hence the results are much deteriorated. Since the modern processors can easily deal with higher computational burden and field-oriented control is feasible in real time, it has been validated by extensive simulations that FOC based IPM drives are superior to their HB-DTC counterparts.

Keywords: FOC, HB-DTC, current distortion, computational burden

[1] Osman Emre ÖZÇİFLİKÇİ (**Orcid ID**: 0000-0001-8770-020X), Mikail KOÇ (**Orcid ID:** 0000-0003-1465-1878), Kırşehir Ahi Evran University, Faculty of Engineering and Architecture, Department of Electrical and Electronics Engineering, Kırşehir,Türkiye

***Corresponding Author:** Osman Emre ÖZÇİFLİKÇİ, e-mail: osman.ozciflikci@ahievran.edu.tr

INTRODUCTION

The excessive use of fossil fuels causes acid rain, global warming, and an increase in the emission of greenhouse gases (Urazel and Keskin, 2020). The transportation sector is one of the dominant sectors in which fossil fuels are widely used (Pongthanaisawan and Sorapipatana, 2013; Can Güven, E. and Gedik, K. 2019; Umar et al., 2021). By reducing the use of fossil fuels in transportation, the increasing acceleration of environmental pollution can be alleviated. Hence, the use of electric vehicles has been increasing and continues to increase in recent years as they reduce fuel comsumption and carbon dioxide emissions (Alyakhni et al., 2021).

Permanent magnet synchronous motors (PMSM) are widely used in industrial applications and electric vehicles due to their superior features such as high power density, high efficiency, high torque density and so on (Ge et al., 2020; Zhang et al. 2021). Interior mounted permanent magnet synchronous motors (IPMs) are a type of PMSMs and they are frequently used in areas such as electric vehicle traction applications (Kim and Seok, 2013) requiring high torque density (Özçiflikçi et al., 2021).

IPMs are generally controlled by two different vector control techniques, namely field oriented control (FOC) and direct torque control (DTC). Although both strategies are in a closed loop manner, the dq- axis current errors are driven to zero with the help of controllers such as PI, in the FOC technique (Zhang et al., 2021). On the other hand, the controlled state variables are the torque and flux in DTC technique where the inverter gates are triggered based on comparisons between observed and command values of the torque and stator flux magnitude values (Li et al., 2021).

The FOC strategy relies on measured phase currents for feedback control and the phase current limits can directly be posed as they are the controlled state variables. Besides, the strategy has started to be implemented for IPM drives several years earlier than the DTC strategy. Thus, the FOC based IPM drives are quite common in the literature. The studies in (Candelo-Zuluaga et al., 2021; Q. Wang et al., 2021) can be given as examples to recent FOC based drives where the parameter variations due to internal and external reasons are handled to improve drive system.

In the meantime, DTC technique is also broadly used in IPM drives as an alternative control strategy and can be divided into two groups as hysteresis-based DTC (HB-DTC) (Shao et al., 2021; Nasr et al., 2022) and pulse width modulation (PWM)-based DTC techniques (X. Wang et al., 2019).. While the HB-DTC technique performs the torque control of the motor using hysteresis comparators and a switching table, the PWM based DTC technique is based on the principle of operating the drive system with a modulation strategy. In early years of DTC drives, the strategy has been implemented with hysteresis bands where the switches are triggered abruptly between two states. Later, PWM based DTC drives have been developed achieving reduced torque ripple (X. Wang et al., 2017). Although less current distortions and smoother output torque can be achieved with PWM based DTC drives, the superior features of HB-DTC drives such as less burden on the processor, eliminating the need for a position sensor, less component in practical system, and simpler implementation due to less complexity of the HB-DTC strategy render them quite common even in recent studies (Mohan et al., 2016; Hakami and Lee, 2020; Xu, Odavic et al., 2021; Ben Mahdhi et al., 2022).

Matrix converter fed drives using multidimensional switching table for common mode voltage minimization has been proposed for HB-DTC drives in (Deng and Li, 2021). (Lin et al.,2020) improves the flux observer structure for HB-DTC drives. A new torque regulator structure is proposed in (X. Wang et al., 2020) to improve the control performance of HB-DTC drives. Transient and steady-state performance of HB-DTC drives have been improved by achieving fast torque response and reduced current distortion in (Bıçak and Gelen, 2021) using seven-level torque hysteresis comparator in a 5-

phase IPM drive. In short, the HB-DTC drives (bang-bang control) are extensively employed in recent IPM drives.

All in all, modern IPM drives can be categorized under FOC, HB-DTC and PWM-DTC each having pros and cons. Hence, the comparisons between the modern control strategies will be inspiring for future trends of IPM drives. The study in (M. Wang et al., 2021) compares different implementation strategies of HB-DTC drives and validates that the control performance can be improved by eliminating the hysteresis bands. Similarly, the proposed HB-DTC drive with 4-dimensional switching table in (Xia et al., 2016) is compared with the standard HB-DTC drive where the deteriorated current and torque waveforms are validated. (X. Wang et al., 2019) compares HB-DTC and PWM-DTC drives in great detail and proposes a hybrid control model. The comparative study between FOC and PWM-DTC has been reported in (Wu et al., 2018).

In this study, the two common control strategies for IPM drives, HB-DTC and the FOC technique are compared in detail by paying particular attention to current distortions, torque ripples and computational burden on microprocessor.

MATERIALS AND METHODS

Mathematical Modelling of IPM Machines

As seen from Figure 1, the electrical expressions in the ABC frame are transformed into $\alpha\beta$ frame with Clarke matrix and then transformed into the d- and q- axes by using Park matrix. (1-3) is obtained when the motor model in ABC frame is transformed into dq-frame based on peak convention (Alışkan and Ünsal, 2018; Koc et al., 2021).

$$V_d = R_s I_d + L_d \frac{dI_d}{dt} - w_e L_q I_q \quad (1)$$

$$V_q = R_s I_q + L_q \frac{dI_q}{dt} + w_e L_d I_d + w_e \psi_m \quad (2)$$

$$T_e = \frac{3p}{2}\left(I_q \psi_m + \left(L_d - L_q\right) I_d I_q\right) \quad (3)$$

V_d and V_q are voltages, I_d and I_q are currents of the direct and quadrature axes, respectively, w_e is the electrical speed in rad/s, p is the pole-pair number, L_d and L_q are the inductance values of the direct and quadrature axes, Ψ_m is the permanent magnet flux linkage and R_s is the stator resistance.

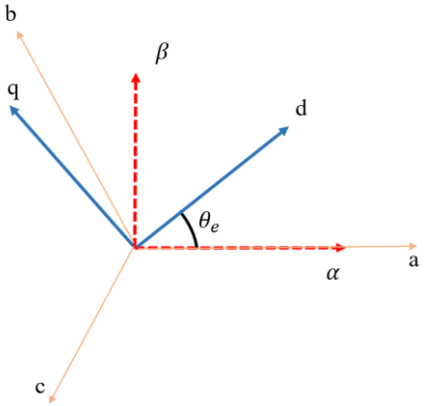

Figure 1. Coordinate Transformations

Implementation of Drive System Simulations

Implementation strategy of the hysteresis based direct torque control and the field oriented controlled IPM drives will be discussed in this section.

HB-DTC Technique

In the HB-DTC technique, the reference torque and flux values are compared with the observed flux and torque. According to the resulting error value, hysteresis bands send a signal to the switching block for switching. According to the look-up table values given in Table 1, gate signals are transmitted to the inverter circuit. The block diagram of the HB-DTC technique is as given in Figure 2.

Table 1. Look-up Table

$d\psi_s$	dT_e	Sector 1	Sector 2	Sector 3	Sector 4	Sector 5	Sector 6
	1	V3	V4	V5	V6	V1	V2
0	0	V0	V7	V0	V7	V0	V7
	-1	V5	V6	V1	V2	V3	V4
	1	V2	V3	V4	V5	V6	V1
1	0	V7	V0	V7	V0	V7	V0
	-1	V6	V1	V2	V3	V4	V5

In the flux and torque observer block, estimation is made according to the voltage and current values received from the inverter output. In (4-8), the equations used to observe flux and torque values are given (Koc et al., 2016). The reason for using $\alpha\beta$-frame for torque and flux observer is that the use of encoder is eliminated. As can be seen from Figure 3, if it is desired to design a torque and flux observer in the dq-frame, rotor position information is required, hence the use of an encoder or resolver becomes essential.

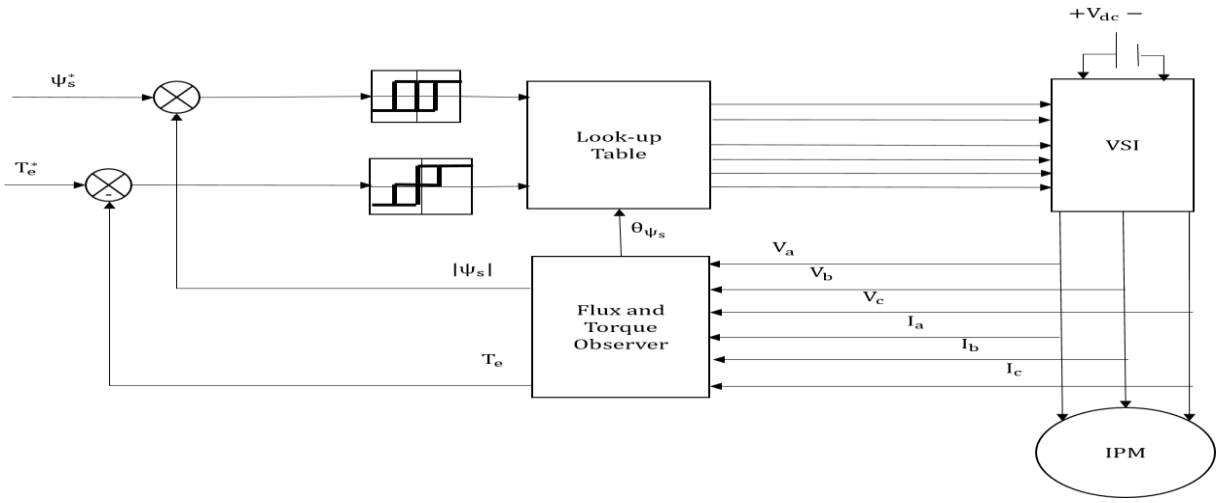

Figure 2. Schematic of HB-DTC Technique

$$\psi_\alpha = \int (V_\alpha - R_s * I_\alpha) dt \tag{4}$$

$$\psi_\beta = \int (V_\beta - R_s * I_\beta) dt \tag{5}$$

$$|\psi_s| = \sqrt{{\psi_\alpha}^2 + {\psi_\beta}^2} \tag{6}$$

$$\theta_{\psi_s} = \tan^{-1} \frac{\psi_\beta}{\psi_\alpha} \tag{7}$$

$$T_e^* = \frac{3 * p}{2} * (\psi_\alpha * I_\beta - \psi_\beta * I_\alpha) \tag{8}$$

The three-phase components obtained from the inverter output are defined on the $\alpha\beta$-frame by means of coordinate transformations. As can be seen from Figure 3, torque and flux values in x and y axes can be easily controlled by using a voltage-based observer. The amplitude of the flux vector is obtained from equation (3) and compared with the command flux value and the flux error is obtained.

The sector information in the look-up table is obtained in terms of the flux vector. The torque value to be compared with the command torque is calculated with (8).

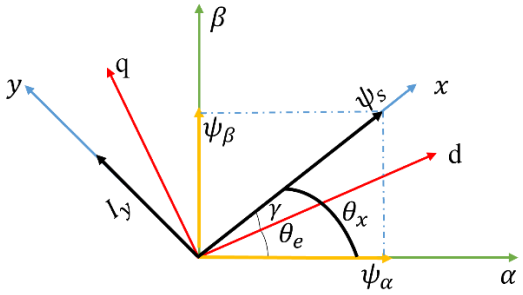

Figure 3. Coordinate Transformations for HB-DTC

FOC Technique

In the FOC technique, a current-based closed-loop control system is created to ensure that the command values are tracked by the driver. According to the schematic given in Figure 4, the three-phase current components measured from the inverter output are defined on the dq-axes with the help of coordinate transformations. Error values are generated for the dq-axes by comparing them with the command dq-axes currents. The resulting error value is driven to zero by PI regulators and voltage commands are generated. In order to drive three-phase motors by FOC technique, a pulse width modulation (PWM) switching strategy is used.

Table 2. Machine Parameters

Motor Type	IPMSM	
Phase Number/ Pole Number	3/8	
Nominal Speed	2500 rpm	@120 V DC
Continuous Torque	15.7 N.m	@51.6 A rms
Continuous Power	4.1 kW	@120 V DC
Input Voltage Range	12V-600V	
Nominal d Axes Inductance	0.282 mH	
Nominal q Axes Inductance	0.828 mH	
Nominal PM Flux Linkage	0.182 Wb	
Nominal Phase Resistance	0.0463 ohm	
Inertia	0.0072 kg.m2	

Space vector pulse width modulation (SVPWM) is the most commonly used strategy in the literature for reasons such as higher DC bus voltage utilization, having less switching loss, and less harmonics (Bingöl and Elmas, 2017; Chokkalingham et al., 2018; Kesler, 2018). As can be seen from Figure 4, it is aimed to model a drive system controlled by PI regulators and using the SVPWM strategy.

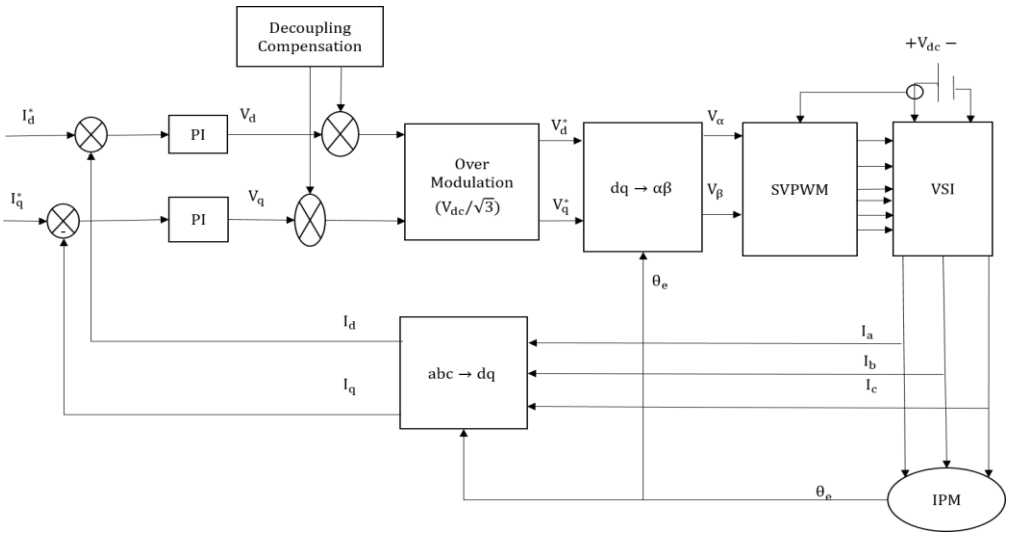

Figure 4. Schematic of FOC Technique

Figure 5. 36-slot 8-pole IPM Machine

RESULTS AND DISCUSSION

Validation of Drive Systems

The HB-DTC technique has been employed on the prototype IPM motor in the simulation environment and the results have been discussed. Machine specifications are listed in Table 2. The view of the prototype machine used in the simulation is illustrated in Figure 5. 36 slot 8-pole machine has been employed. The results have been obtained by keeping the hysteresis band gaps at 5% of the continuous torque value for the torque comparator and 5% of the magnet flux linkage value for the flux comparator.

As can be seen from Figure 6, the speed has been increased from 0 rpm to 2000 rpm in order to test the drive system at different operating points. The stability of the drive system is achieved in the transient state by step changing the command torque. In addition, in the case where the mechanical speed is constant, the electromagnetic torque value is changed with the step function, and its stability in the steady state is also achieved. As a result, it has been validated that the drive system tracks the command values at different operating points. However, when the electromagnetic torque command is 5 Nm at low speeds (0-250 rpm), as can be seen from Figure 6, performance of the control system degrades. This is as expected as the flux observer performance utilizing (4) and (5) degrades at low frequencies.

Figure 7 compares the ripples at the output torque when the hysteresis band gaps are 5%, 10% and 20% of the continuous torque and nominal magnetic flux linkage value when the mechanical speed is 1000 rpm. Three drive systems have been operated with different hysteresis bandwidths. As can be deduced, the torque ripple can be further reduced by reducing the hysteresis bandwidth.

The command values applied to the machine with the HB-DTC technique has been applied to the machine with FOC technique and the results are illustrated in Figure 8. It is evident from Figure 8 that stable control has also been achieved with FOC strategy as well. The switching frequency is set to 5 kHz. It is evident from Figures 6 and 8 that while the drive performance degrades at low speeds, the FOC based drive achieves better performance.

Comparison of THD Ratios and Current Distortions

In this section, THD analyzes in wide frequency range are compared for both control strategies. The drive systems should be run at the similar switching frequencies for a fair comparison. Since the switching frequency of the HB-DTC technique is variable, while the mechanical speed value is 1000 rpm and the electromagnetic torque value is 10 Nm, the average switching frequencies are determined by changing the bandwidth from 1% to 30%. As given in Figure 9, average switching frequency values for varying bandwidths has been obtained for the HB-DTC technique.

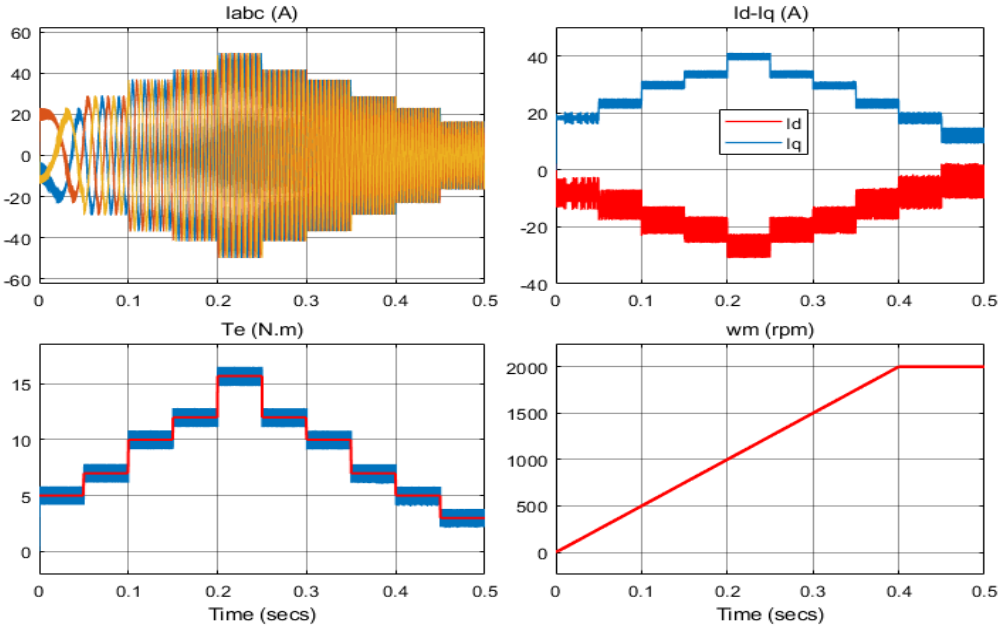

Figure 6. Validation of HB-DTC

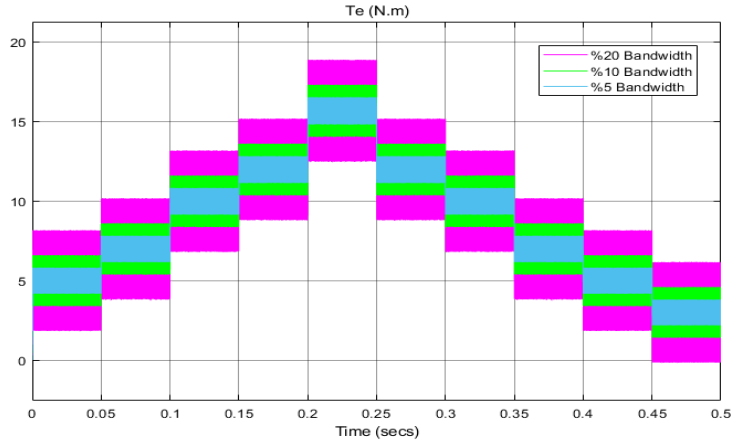

Figure 7. Torque Outputs with Different Bandwidths (Torque:15.7*Bandwidth-Flux:0.0182*Bandwidth)

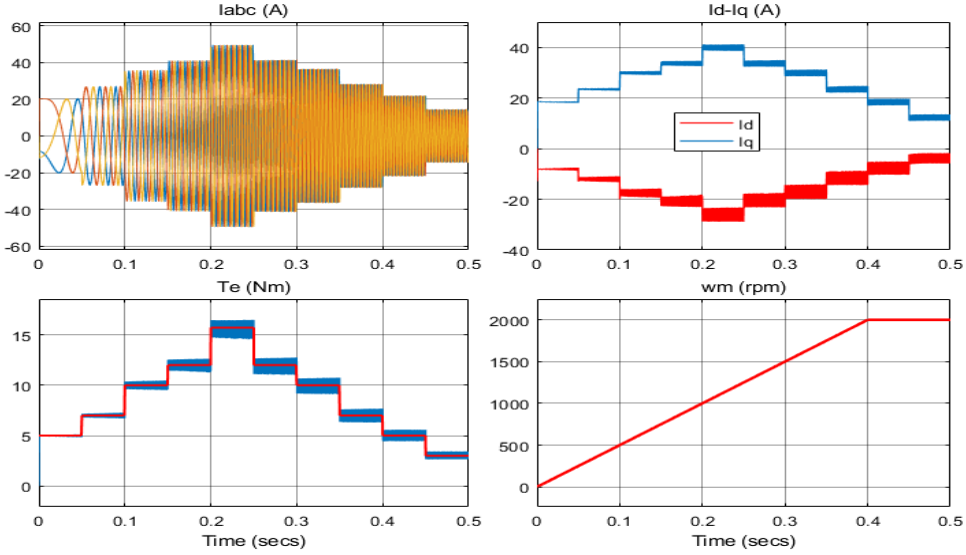

Figure 8. Validation of FOC Technique

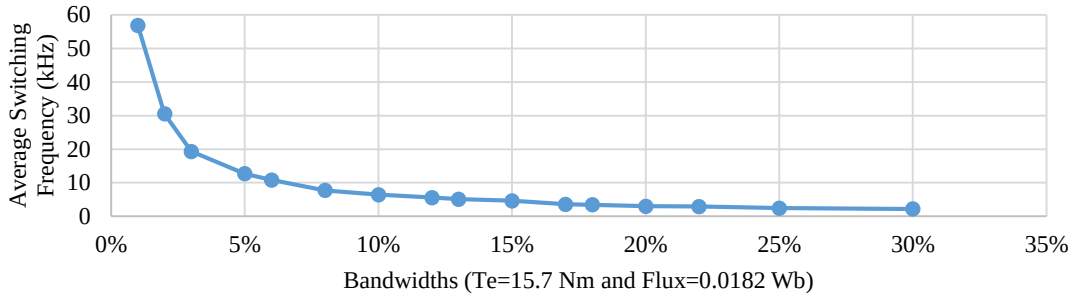

Figure 9. Average Switching Frequency of HB-DTC Technique

Figure 10(a) gives the THD ratios that occur when the motor with FOC drive is controlled with different switching frequencies. SVPWM switching strategy has superior features such as low switching losses and low harmonic distortions, and hence it is the most commonly used modulation strategy. Thus, it has been adopted in this study. In addition, in the HB-DTC technique, THD ratios have been obtained when the motor is operated at 10 Nm load and 1000 rpm mechanical speed. The results with FOC strategy has been obtained at a wide switching frequency range between 1 kHz and 40 kHz. As a result, even at the lowest switching frequency of 1 kHz, the THD ratio on the current is 5.85%. Also, the THD ratio is 2.26% at 10 kHz switching frequency.

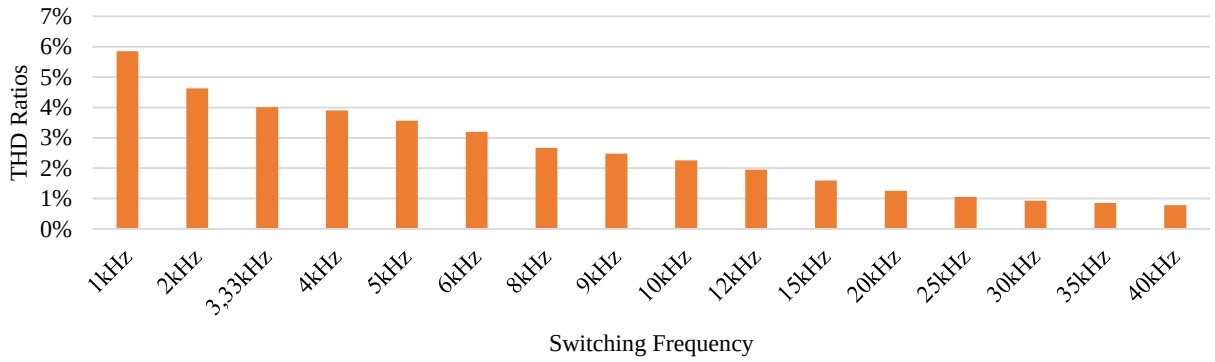

(a)

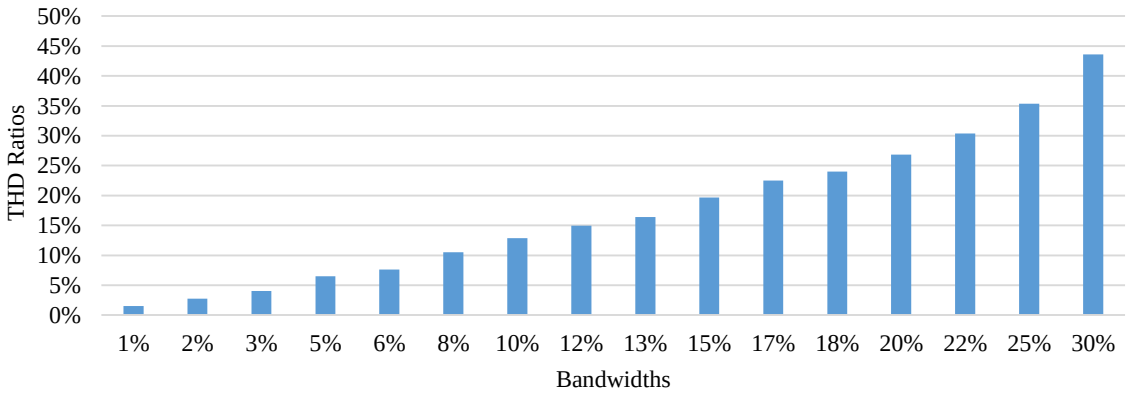

(b)

Figure 10. (a) THD Ratios of FOC Drive (b) THD Ratios of HB-DTC Drive

In Figure 10(b), THD results are obtained by varying bandwidths of the hysteresis comparators in the HB-DTC technique. In order to operate at the same switching frequency with the FOC technique, a comparison can be made with the transition between the bandwidth in Figure 9 and the average switching frequency. First, Figure 10(b) has been obtained to see the effects of bandwidths on the current THD.

According to Figure 10(b), the current THD ratio in the HB-DTC drive with 1% and 30% bandwidth hysteresis comparators is between 1.55% and 43.61%, respectively. The fact that the hysteresis band is at the level of 6% corresponds to a THD ratio of 7.64% on the current. Accordingly, for the 10 kHz frequency value, there is a THD ratio of 2.26% in the FOC technique, while this rate is 7.64% in HB-DTC. THD comparisons of FOC and HB-DTC techniques at different switching frequencies are given in Table 3.

Table 3. Comparisons of THD Ratios Between FOC and HB-DTC Techniques

Average Switching Frequency	FOC	HB-DTC
2 kHz	4.63%	43.61%
3.3 kHz	4.01%	24.03%
5 kHz	3.57%	16.43%
10 kHz	2.26%	7.64%
12 kHz	1.95%	6.52%
20 kHz	1.25%	4.06%
30 kHz	0.93%	2.75%

According to Table 3, it has been validated that the system with FOC controlled drive is quite superior to the HB-DTC technique in terms of THD. The THD ratio when the HB-DTC technique operates at a switching frequency of 30 kHz is close to the THD ratio when the FOC technique operates at around 10 kHz.

In Figure 11, while the bandwidth of the HB-DTC technique is 13%, that is, with an average switching frequency of 5 kHz, the FOC technique is operated at the same switching frequency and the ripple on the output torque is illustrated. While comparing both techniques, the mechanical speed and the electromagnetic torque commands are the same which are 1000 rpm and 15.7 Nm, respectively. As it is evident in Figure 11 that the torque ripple ratio when FOC technique is adopted is 4.38%, while it is 11.75% when HB-DTC is adopted. In addition, when the same torque-speed profile is applied, the waveforms of the output phase currents of both techniques are depicted in Figure 11. As can be seen, the difference between torque ripple and current distortions is reasonably higher with HB-DTC drive as can also be deduced from THD comparisons.

As a result of THD ratios, torque ripples and current distortions, the FOC technique is quite superior to HB-DTC technique. As for the computational burden on the processors, Figure 12 compares the two drives. In order for a fair comparison, all irrelevant or less relevant elements have been removed from the simulations unless the elements are mandatory. Drives have been operated on a computer with i5 CPU and 2.9 GHz processor for simulation of 10 seconds in real time. The drives are operated at the continuous torque at 1000 rpm speed. As can be seen from Figure 12, the computational burden on the processor is lower when the HB-DTC technique is adopted. While HB-DTC technique achieves to complete the simulation in 349 sec, FOC technique operates on the same profile and completes it in 428 sec.

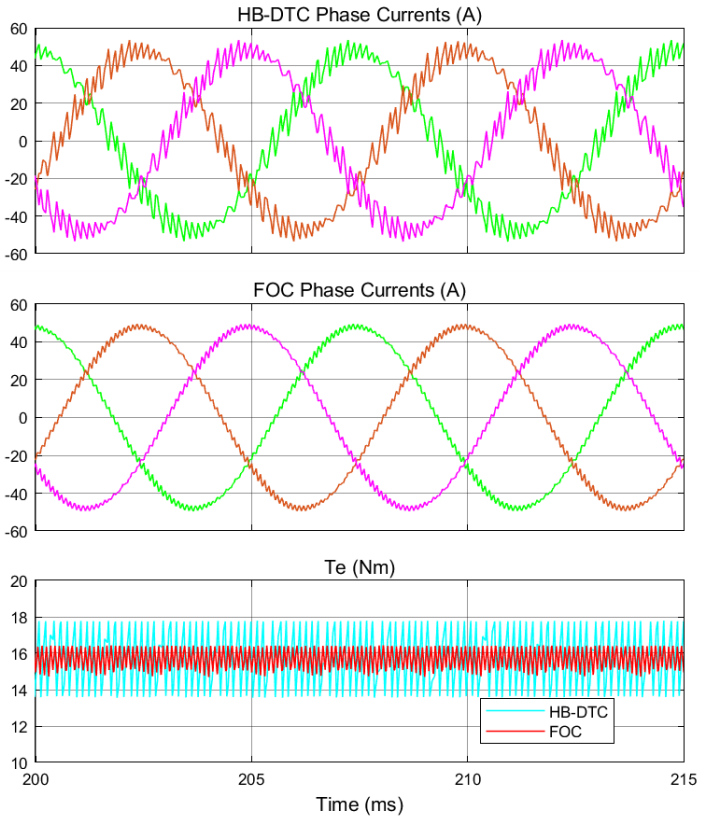

Figure 11. Comparison of Torque Ripple

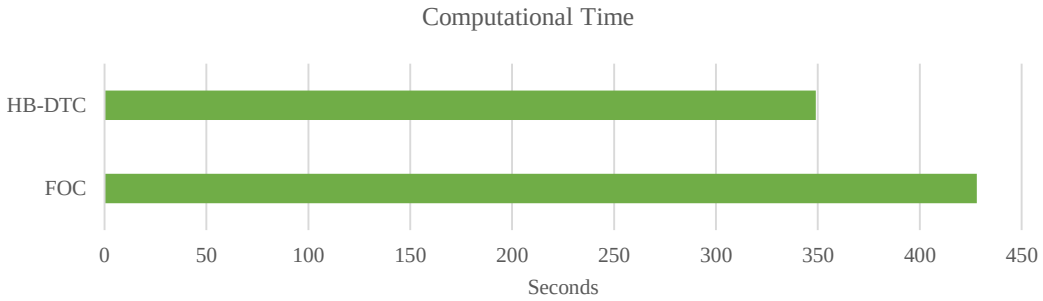

Figure 12. Comparison of Computational Burden

CONCLUSION

In this study, the HB-DTC and the FOC techniques, which are extensively used in modern drives, have been comprehensively compared in particular attention to output current distortions, THD ratios, torque ripples and computational burden. The average switching frequency value of the HB-DTC technique is altered by changing the bandwidth of the torque and flux hysteresis comparators. In order to achieve fair comparisons, the average switching frequency of the HB-DTC drives have been obtained and irrelevant elements have been removed from the simulated drives. The simulation results validate the overwhelming superiority of the FOC based drives in terms of current distortions, THD ratios and torque ripples. However, the results also validate that the burden on the processor is less when HB-DTC drive is employed. Considering all, the HB-DTC drives are superior considering the burden on the processer and they have less component as there is no position sensor but the current waveforms are much distorted and hence increased torque ripples.

ACKNOWLEDGEMENTS

This study has been supported by the Scientific and Technological Research Council of Turkey (TUBITAK) through the Scientific and Technological Research Projects Funding Program (1001) with a project numbered as 118E858.

Conflict of Interest

The article authors declare that there is no conflict of interest between them.

Author's Contributions

The authors declare that they have contributed equally to the article.

REFERENCES

Alışkan İ, Ünsal S, 2018. Speed control of permanent magnet synchronous motor by using fuzzy logic controllers having different inference methods. Pamukkale University Journal of Engineering Sciences, 24(2), 185-191.

Alyakhni A, Boulon L, Vinassa J. M, Briat O, 2021. A Comprehensive Review on Energy Management Strategies for Electric Vehicles Considering Degradation Using Aging Models. IEEE Access, 9, 143922-143940.

Ben Mahdhi H, Ben Azza H, Jemli M, 2022. Inverter open-circuit fault diagnosis method in PMSG based wind energy conversion system. Electrical Engineering, 104(3), 1317-1330.

Bıçak A,Gelen A, 2021. Sensorless direct torque control based on seven-level torque hysteresis controller for five-phase IPMSM using a sliding-mode observer. Engineering Science and Technology, an International Journal, 24(5), 1134-1143.

Bingöl O, Elmas C, 2017. Virtual lab: Space vector PWM for two-and three-level inverters. Pamukkale University Journal of Engineering Sciences, 23, 95-102.

Can Güven E, Gedik K, 2019. Ömrünü Tamamlamış Elektrikli Araç Bataryalarının Çevresel Yönetimi . Journal of the Institute of Science and Technology , 9 (2) , 726-737 .

Candelo-Zuluaga C, Riba J. R, Garcia A, 2021. PMSM Parameter Estimation for Sensorless FOC Based on Differential Power Factor. IEEE Transactions on Instrumentation and Measurement, 70, 1-12.

Chokkalingham, B, Padmanaban, S, Blaabjerg F, 2018. Investigation and Comparative Analysis of Advanced PWM Techniques for Three-Phase Three-Level NPC-MLI Drives. Electric Power Components and Systems, 46(3), 258-269.

Deng W, Li S, 2021. Direct Torque Control of Matrix Converter-Fed PMSM Drives Using Multidimensional Switching Table for Common-Mode Voltage Minimization. IEEE Transactions on Power Electronics, 36(1), 683-690.

Ge Y, Yang L, Ma X, 2020. Adaptive sliding mode control based on a combined state/disturbance observer for the disturbance rejection control of PMSM. Electrical Engineering, 102(4), 1863-1879.

Hakami S, Lee K.-B, 2020. Four-Level Hysteresis-Based DTC for Torque Capability Improvement of IPMSM Fed by Three-Level NPC Inverter. Electronics, 9, 1558.

Kesler S, 2018. Performance Analysis of Different PWM Techniques on V/f-based Speed Control with Boost Voltage Application for Induction Motors. Pamukkale University Journal of Engineering Sciences, 24, 797-808.

Kim S, Seok J, 2013. Maximum Voltage Utilization of IPMSMs Using Modulating Voltage Scalability for Automotive Applications. IEEE Transactions on Power Electronics, 28(12), 5639-5646.

Koc M, Sun T, Wang J, 2016. Performance improvement of direct torque controlled interior mounted permanent magnet drives by employing a linear combination of current and voltage based flux observers. IET Power Electronics, 9(10), 2052-2059.

Koc M, Emiroglu S, Tamyürek B, 2021. Analysis and simulation of efficiency optimized IPM drives in constant torque region with reduced computational burden. Turk J Elec Eng & Comp Sci, 29, 1643 – 1658.

Li H, Wang Z, Xu Z, Wang X, Hu Y, 2021. Feedback Linearization Based Direct Torque Control for IPMSMs. IEEE Transactions on Power Electronics, 36(3), 3135-3148.

Lin X, Huang W, Jiang W, Zhao Y, Zhu S, 2020. A Stator Flux Observer With Phase Self-Tuning for Direct Torque Control of Permanent Magnet Synchronous Motor. IEEE Transactions on Power Electronics, 35(6), 6140-6152.

Mohan D, Zhang X, Foo G. H. B, 2016. Three-Level Inverter-Fed Direct Torque Control of IPMSM With Torque and Capacitor Voltage Ripple Reduction. IEEE Transactions on Energy Conversion, 31(4), 1559-1569.

Nasr A, Gu C, Wang X, Buticchi G, Bozhko S, Gerada C, 2022. Torque-Performance Improvement for Direct Torque-Controlled PMSM Drives Based on Duty-Ratio Regulation. IEEE Transactions on Power Electronics, 37(1), 749-760.

Özçiflikçi OE, K. M, Bahçeci S, 2021. Maximum Torque per Ampere Strategy in IPM Drives for Electric Vehicles. El-Cezeri, 8(3), 1405-1415.

Pongthanaisawan J, Sorapipatana C, 2013. Greenhouse gas emissions from Thailand's transport sector: Trends and mitigation options. Applied Energy, 101, 288-298.

Shao B, Zhu Z. Q, Feng J, Guo S, Li Y, Liao W, 2021. Compensation of Selective Current Harmonics for Switching-Table-Based Direct Torque Control of Dual Three-Phase PMSM Drives. IEEE Transactions on Industry Applications, 57(3), 2505-2515.

Umar M, Ji X, Kirikkaleli D, Alola A. A, 2021. The imperativeness of environmental quality in the United States transportation sector amidst biomass-fossil energy consumption and growth. Journal of Cleaner Production, 285, 124863.

Urazel and Keskin, 2020, Electric Drive Vehicle Model and Simulation with MATLAB. Journal of the Institute of Science and Technology. 10(4): 2461-2473.

Wang M, Sun D, Zheng Z, Nian H, 2021. A Novel Lookup Table Based Direct Torque Control for OW-PMSM Drives. IEEE Transactions on Industrial Electronics, 68(10), 10316-10320.

Wang Q, Wang G, Zhao N, Zhang G, Cui Q, Xu D, 2021. An Impedance Model-Based Multiparameter Identification Method of PMSM for Both Offline and Online Conditions. IEEE Transactions on Power Electronics, 36(1), 727-738.

Wang X, Wang Z, Cheng M, Hu Y, 2017. Remedial Strategies of T-NPC Three-Level Asymmetric Six-Phase PMSM Drives Based on SVM-DTC. IEEE Transactions on Industrial Electronics, 64(9), 6841-6853.

Wang X, Wang Z, Xu Z, 2019. A Hybrid Direct Torque Control Scheme for Dual Three-Phase PMSM Drives With Improved Operation Performance. IEEE Transactions on Power Electronics, 34(2), 1622-1634.

Wang X, Wang Z, Xu Z, Cheng M, Hu Y, 2020. Optimization of Torque Tracking Performance for Direct-Torque-Controlled PMSM Drives With Composite Torque Regulator. IEEE Transactions on Industrial Electronics, 67(12), 10095-10108.

Wu B, Xu D, Ji J, Zhao W, Jiang Q, 2018. Field-oriented control and direct torque control for a five-phase fault-tolerant flux-switching permanent-magnet motor. Chinese Journal of Electrical Engineering, 4(4), 48-56.

Xia C, Wang S, Wang Z, Shi T, 2016. Direct Torque Control for VSI–PMSMs Using Four-Dimensional Switching-Table. IEEE Transactions on Power Electronics, 31(8), 5774-5785.

Xu J, Odavic M, Zhu Z. Q, Wu Z. Y, Freire N, 2021. Switching-Table-Based Direct Torque Control of Dual Three-Phase PMSMs With Closed-Loop Current Harmonics Compensation. IEEE Transactions on Power Electronics, 36(9), 10645-10659.

Zhang Y, Jin J, Huang L, 2021. Model-Free Predictive Current Control of PMSM Drives Based on Extended State Observer Using Ultralocal Model. IEEE Transactions on Industrial Electronics, 68(2), 993-1003.

hang Y, Yin Z, Bai C, Wang G, Liu J, 2021. A Rotor Position and Speed Estimation Method Using an Improved Linear Extended State Observer for IPMSM Sensorless Drives. IEEE Transactions on Power Electronics, 36(12), 14062-14073.